# Exploring parameter constraints on quintessential dark energy: The inverse power law model

Mark Yashar, Brandon Bozek, Augusta Abrahamse, Andreas Albrecht, and Michael Barnard

*Department of Physics, University of California at Davis, One Shields Avenue, Davis, California 95616, USA*

(Received 17 November 2008; published 7 May 2009)

We report on the results of a Markov chain Monte Carlo analysis of an inverse power law (IPL) quintessence model using the Dark Energy Task Force (DETF) simulated data sets as a representation of future dark energy experiments. We generate simulated data sets for a ΛCDM background cosmology as well as a case where the dark energy is provided by a specific IPL fiducial model, and present our results in the form of likelihood contours generated by these two background cosmologies. We find that the relative constraining power of the various DETF data sets on the IPL model parameters is broadly equivalent to the DETF results for the $w_0 - w_a$ parametrization of dark energy. Finally, we gauge the power of DETF "stage 4" data by demonstrating a specific IPL model which, if realized in the universe, would allow stage 4 data to exclude a cosmological constant at better than the $3\sigma$ level.

DOI: 10.1103/PhysRevD.79.103004 PACS numbers: 95.36.+x, 98.80.Es

## I. INTRODUCTION

A host of cosmological measurements indicate that the universe is undergoing a phase of accelerated expansion. This has been generally attributed to a significant component of smooth energy with a large negative pressure, referred to as dark energy (DE) and characterized by an equation-of-state parameter $w \equiv \frac{p}{\rho}$. Current measurements indicate that about 70% of the density of the universe today is comprised of this dark energy. Candidates for DE include a cosmological constant $\Lambda$ and a slowly evolving dynamical scalar field such as quintessence [1]. In quintessence models, the cosmic acceleration is driven by a scalar field $\phi$ slowly evolving in some potential $V(\phi)$. In this scenario, the parameters of the potential $V(\phi)$ determine the properties of the dark energy.

In general, all DE models have serious unresolved theoretical problems, and one can make the case in different ways as to which types, if any (i.e. $\Lambda$ or quintessence DE), are best motivated [2,3]. This paper is motivated by the fact that scalar field quintessence is definitely part of the theoretical discussion, and thus it should also be part of the process whereby we evaluate future dark energy experiments. This paper is the fifth in a series of papers motivated in this way [4–7]. The inverse power law (IPL) model we consider here is one of the more popular quintessence models. One of its attractive features is its "tracking" behavior that makes its predictions independent of the initial conditions for $\phi$, assuming that $\phi$ starts out in the (rather broad) basin of attraction for tracking. Also, the behavior of the equation of state in the IPL model tends to be quite different than for the models considered in our previous work (see [7] for a unified discussion), so this makes it an interesting complement to our other work.

Recently, the Dark Energy Task Force (DETF) produced a report that considered the impact of various projected data sets (referred to as "data models" and representing future DE observations) on cosmological parameters in a standard ΛCDM cosmological model using the "$w_0 - w_a$" parametrization of the dark energy equation of state [8], $w(a) = w_0 + w_a(1 - a)$, where the scale factor $a = 1$ today [9–11]. They assessed the impact of a given data set using a "figure of merit" (FoM), defined as the inverse of the area inside the 95% confidence contour in the $w_0 - w_a$ plane for a fiducial ΛCDM model. However, as has been pointed out by a number of authors (e.g., [12]), the two-parameter $w_0 - w_a$ phenomenological model is not motivated by an actual physical model of dark energy and exhibits very different behavior compared with popular dark energy models. More recently, the Joint Dark Energy Mission Figure of Merit Science Working Group (JDEM FoMSWG) [13] has expanded and improved upon the work of the DETF by developing a means for measuring the constraining power of a dark energy experiment that includes a principal-components approach involving the redshifts at which each experiment has the power to constrain $w$. Our work (represented by this and our companion papers [4–6]) supplements the work of the DETF and JDEM FoMSWG by assessing the capability of future experiments to constrain DE by using an equation-of-state parametrization that *is* motivated by a physical model of DE—the well-known IPL quintessence model. This potential has its own motivations, and is also included here because it generates a family of functions $w(a)$ that are quite different than those considered in our other work. Our work also complements the work of [14,15], which consider generalized classes of scalar field potentials.

This paper is organized as follows. In Sec. II we describe the features of the IPL quintessence model and its tracking properties. While most of the focus of this paper is on the tracking behavior of the IPL model, we also briefly discuss the nontracking transient and "thawing" behaviors of this model. In Sec. III we describe how we parametrize the IPL model for our Markov chain Monte Carlo (MCMC) analysis. In Sec. IV B we present our MCMC analysis and results using data forecast by DETF to constrain the IPL

 

quintessence model around a fiducial ΛCDM model. In Sec. IV C we give our MCMC analysis for simulated data generated from a fiducial IPL model. This allows us to further ascertain how sensitive future observations may be to deviations from a cosmological constant, and to assess to what extent we can exclude the Λ model if IPL quintessence occurs in nature. In Sec. IV D we briefly discuss our MCMC analysis of nontracking regions of parameter space. Finally, we discuss our results and present our conclusions in Sec. V.

## II. TRACKING QUINTESSENCE

For a homogeneous scalar field in a Friedmann-Robertson-Walker universe, the evolution of the scalar field, given by its equation of motion, is described by the Klein-Gordon equation

$$\ddot{\phi} + 3H\dot{\phi} + \frac{dV}{d\phi} = 0 \tag{1}$$

where the Hubble parameter $H$ is given by the Friedmann equation (with $\phi$ and spatial curvature also taken into account here)

$$H^2 = \left(\frac{\dot{a}}{a}\right)^2 = \frac{1}{3M_P^2}(\rho_r + \rho_m + \rho_\phi) - \frac{k}{a^2}, \tag{2}$$

where $a$ is the scale factor, $M_P \equiv 8\pi G^{-(1/2)}$ is the reduced Planck mass, $\rho_r(a)$ is the radiation background energy density, $\rho_m(a)$ is the matter background energy density, $\rho_\phi(a)$ is the scalar field energy density, and $k$ is the curvature constant. The energy density and pressure of the scalar field are

$$\rho_\phi = \tfrac{1}{2}\dot{\phi}^2 + V(\phi), \tag{3}$$

$$p_\phi = \tfrac{1}{2}\dot{\phi}^2 - V(\phi), \tag{4}$$

where the dots denote derivatives with respect to time. Equations (1)–(4) enable us to solve for the background evolution in a quintessence cosmology, once the potential $V(\phi)$ and energy densities of the different components, $\rho_m$, $\rho_r$, etc., have been assigned. If the scalar field rolls slowly enough such that the kinetic energy density is much less than the potential energy density, i.e., the slow-roll limit, $\dot{\phi}^2 \ll V(\phi)$, then the pressure $p_\phi$ of the scalar field will become negative and the field energy will approximate the effect of a cosmological constant. This indicates that a flat potential $V(\phi)$ is required to give rise to accelerated expansion [16]. This slow-roll limit corresponds to $w_\phi = -1$ and $\rho_\phi = \text{const}$. It also follows that the equation of state of quintessence is bounded in the range $-1 < w_\phi < 1$ and is usually nonconstant. In these models, the dark energy behaves as a perfect fluid in which the equation of state,

$$w \equiv \frac{p_\phi}{\rho_\phi} = \frac{\frac{1}{2}\dot{\phi}^2 - V(\phi)}{\frac{1}{2}\dot{\phi}^2 + V(\phi)}, \tag{5}$$

changes with time and is typically negative when $V(\phi)$ is sufficiently dominant, as expected during the recent epoch of accelerated expansion. We can see from Eq. (5) that $\dot{\phi} = 0$ corresponds to the limit in which the scalar field is a cosmological constant with $w_\Lambda = -1$.

### A. Tracking solutions and behaviors

It has been demonstrated [17,18] that a subclass of quintessence potentials, including the IPL potential, have several desirable properties. These include the fact that the equations of motion of these quintessence models have attractor-like solutions in the space of trajectories of $\phi$ (called "tracking" solutions). A broad set of initial conditions $\phi_I$ and $\dot{\phi}_I$ in the early universe (referred to as a "basin of attraction") evolve toward a common attractor solution giving the same late time evolution of $\phi$, and thus allowing the scalar field to induce the present phase of accelerated cosmic expansion starting from a large range of initial conditions. The tracking solutions are characterized by an almost constant $w_\phi$, constrained by $-1 < w_\phi < w_B$, where $w_B$ is the equation of state of the dominating background fluid component. The tracking behavior allows the value of the accelerating matter density today to be determined by parameters in the quintessence potential, largely independent of the scalar field initial conditions [19]. We note, however, that although this behavior may help to explain why the dark energy has come to dominate in recent times rather than some earlier epoch, it does not solve the "cosmological constant problem," especially as it relates to the zero point energy of the quantum vacuum.

In [18], a function

$$\Gamma \equiv \frac{V''V}{(V')^2} \tag{6}$$

(where the primes denote derivatives with respect to $\phi$) was defined for determining whether a particular potential admits tracker solutions. It was shown that tracking behavior occurs when either of the following two conditions is met: (a) $\Gamma > \frac{5}{6}$, $w_\phi < w_B$, $\Gamma \approx \text{const}$ (and thus $|\frac{V'}{V}|$ decreases as $V$ decreases) or (b) $\Gamma < 1$, $\frac{1}{2}(1 + w_B) > w_\phi > w_B$, $\Gamma \approx \text{const}$ (and thus $|\frac{V'}{V}|$ is strictly increasing as $V$ decreases). The only constraint on the initial energy density in the tracker is that it be less than or equal to $\rho_{B,I}$, the initial energy density of the background fluid component (matter or radiation), and greater than $\rho_{m,0}$, the current matter energy density. This condition is necessary in order for $\phi$ to converge to the tracker solution before the present time [18,20]. On the other hand, solutions of the Klein-Gordon equation do not converge to tracker solutions for potentials in which $w_\phi < w_B$ and $|\frac{V'}{V}|$ strictly increases as $V$ decreases ($\Gamma < 1$), or, equivalently, when $\Gamma < 1 -$

$\frac{(1-w_B)}{6+2w_B}$. Note that $|\frac{V'}{V}|$ gives the slope of the potential. The quantity $\frac{V'}{V}$ is also known as a "slow-roll parameter" (e.g., [10]) which relates to how fast the field moves in the potential for so-called "slow-roll" solutions. One upshot of the above analysis is that one can see that potentials (such as IPL) tend not to have tracking solutions when and where they are flat (that is, where $V'' = V' = 0$).

### B. The inverse power law potential

One of the earliest proposed, simplest, and most widely investigated scalar field quintessence model is the pure inverse power law (IPL) model, originally introduced by Ratra and Peebles [1]. This model was originally put forward to mimic a time-varying cosmological constant undergoing dissipationless decay and is motivated by supersymmetric QCD (see [21] and references therein). More recently, this potential has been reanalyzed [17,18] in the context of a scalar field potential driving the current epoch of cosmic acceleration.

The IPL scalar field potential is self-interacting, minimally coupled to gravity, and given by

$$V = V_0\left(\frac{M_P}{\phi}\right)^{\alpha}. \tag{7}$$

Values of $V_0$ of order the critical density $\rho_c = 3H_0^2M_P^2$ and $\alpha = O(1)$ yield cosmological solutions in which the scalar field can account for the observed cosmic acceleration today [and typically has current values $\phi = O(M_P)$]. Furthermore, a large range of cosmologically realistic solutions exhibit tracking behavior whereby, after some initial transient period, many different solutions lock on to the same attractor solution. This causes the initial conditions for $\phi$ to be irrelevant for predicting observable cosmological features and removes the need for tuning of initial conditions seen in many other quintessence models.

It has been shown that the following relation is maintained on the attractor solutions [1,17,22]:

$$\frac{d^2V}{d\phi^2} = \frac{9}{2}\frac{\alpha(1+\alpha)}{\alpha}(1-w_\phi^2)H^2. \tag{8}$$

The second derivative of the potential gives the scalar field mass which today is given by $m_\phi = V''(\phi_0) \approx \frac{\rho_\phi}{\phi^2}$. The tiny value of this mass ($m_\phi \sim 10^{-33}$ eV) is due to the requirements that $V(\phi)$ slowly varies with the field value and that the current value of $V(\phi)$ be consistent with observations [22]. When the scalar field potential is about to dominate, we use Friedmann's equation, $H^2 \sim \frac{V}{M_P^2}$. Then, if $w_\phi$ and $\alpha$ are of order unity, Eq. (8) indicates that the value of the quintessence field at the present time is of order of the Planck mass [23].

The power law index $\alpha > 0$ determines the shape of the potential as well as the value of $w_\phi$ today. The slope and curvature of the IPL potential are given by

$$\frac{dV}{d\phi} = -\frac{\alpha}{\phi}V(\phi) \tag{9}$$

and

$$\frac{d^2V}{d\phi^2} = \frac{\alpha(1+\alpha)}{\phi^2}V(\phi). \tag{10}$$

We can see that smaller $\alpha$'s lead to a more flat potential, which will in turn lead to more slowly evolving behavior for $\phi$ (and thus values of $w_\phi$ closer to $-1$). Larger values of $\alpha$ lead to a steeper potential slope, causing more evolution for $\phi$ and its energy density, and also values of $w_\phi$ larger than $-1$.

Smaller values of $\phi_I$ as well as larger values of $\alpha$ lead to a steeper initial potential slope and larger values of $V(\phi_I)$. This means that the scalar field will start rolling from higher up on the potential and will roll faster, even for cases where the dark energy is initially dominant and $\alpha$ is correspondingly large, leading to greater evolution of the dark energy density. The quantities $V_0$ and $\alpha$ are the two free parameters in the potential. In some supersymmetric QCD realizations of the IPL model [21], $\alpha$ is also related to the number of flavors and colors, and can take on a continuous range of values $\alpha > 0$ [24]. For $\alpha \rightarrow \infty$ (but with $\rho_\phi$ still subdominant), the scalar field energy density scales like that of the dominant background. Potentials of this type also possess the following phenomenological property: they yield $w_\phi$ values which automatically decrease to negative values at the beginning of matter domination [25]. Given that the energy density of each component evolves as

$$\rho_i \propto a^{-3(1+w_i)} \tag{11}$$

(with $i$ standing for the radiation, matter, or scalar field component), quintessence will eventually come to dominate the universe even if it begins as a subdominant constituent.

The IPL potential is one of a large class of quintessence models with what has been referred to as "runaway scalar fields" [17,20] whose tracker solutions begin from some initial $\phi_I$ and $\dot{\phi}_I$ and share some of the following general features: The field rapidly converges to a point on the potential where $V'' \approx H^2$, where the Hubble parameter $H$ is determined by $\rho_m$ and $\rho_r$. As the universe expands and $H$ decreases, $\phi$ moves down the potential so as to maintain the condition $V'' \approx H^2$. The universe enters a tracking phase where $\rho_\phi$ catches up to the background density $\rho_B$ when $m_\phi^2$ decreases to of order $H^2$ and so $\phi_0 \sim M_P$ [16,18]. Thus, the distinctive feature of these tracker fields is that the evolution of the scalar fields is controlled by $\rho_m$ and $\rho_r$ rather than evolving independently according to its own potential. This controlled evolution continues until $\phi$ finally surpasses the point where critical damping via Hubble expansion occurs. Then the field's own potential energy is sufficient to freeze the field and cause $\rho_\phi$ to

eventually overtake $\rho_m$ and $\rho_r$, driving the universe into a phase of cosmic acceleration.

Figure 1 illustrates how the shape of the IPL potential is changed by selecting three different $\alpha$ values for a fixed $V_0$. The value of $\phi_I$ determines where on the potential the scalar field starts to evolve. The present field value $\phi_0$, of order of the Planck mass $M_P$, is reached from a broad range of initial conditions $\phi_I$ and $\dot{\phi}_I$, with the only important condition being that $\phi_I \ll M_P$ [26], which is consistent with the discussion concerning tracking in Sec. II A and the more detailed discussion and criteria regarding attractor solutions given in [17,18]. The lower panel of Fig. 1 shows the corresponding evolution of the equation of state. For fixed values of $\phi_I$ and $V_0$, we see that larger values of $\alpha$ correspond to $w$ curves with larger amplitudes and which have larger values today, i.e., deviate more from a cosmological constant ($w = -1$) at the present time. As $\alpha \to 0$,

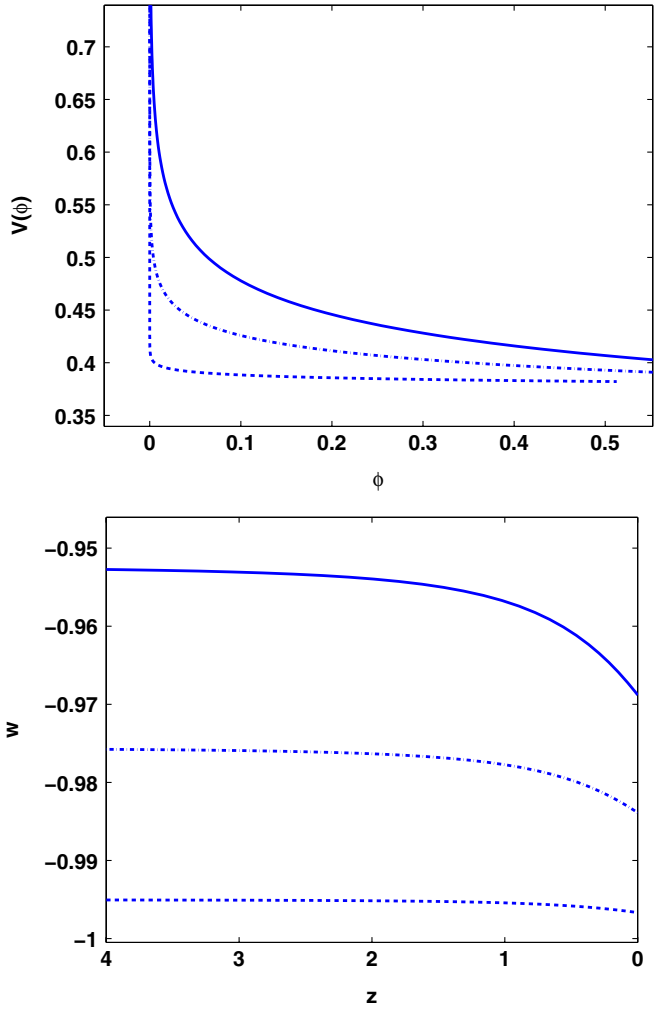


FIG. 1 (color online). IPL potentials (top panel) and $w(z)$ evolution (lower panel) for different $\alpha$ values (dashed-dotted line: $\alpha = 0.05$; dashed line: $\alpha = 0.01$; and solid line: $\alpha = 0.1$). For all curves $V_0 = 0.38$ and $\phi_I = 10^{-30}$. Smaller values of $\alpha$ lead to flatter potentials and smaller $V(\phi)$.

the equation of state more and more mimics the behavior of $\Lambda$ at late times with $w \to -1$. The IPL model has been categorized by [27] as a "cooling" or "freezing" model in which $w > -1$ initially but with $w$ then decreasing towards $-1$ as the scalar field rolls down the potential.

For cases in which radiation or matter is dominant and the contribution of $\rho_\phi$ to the expansion of the universe is neglected, the Klein-Gordon equation gives exact tracking solutions for the evolution of $\phi$ for the IPL model, as well as the following time-independent relations between $\Gamma$, the power law index $\alpha$, and the equation-of-state parameter [17,18],

$$w_\phi = \frac{w_B - 2(\Gamma - 1)}{1 + 2(\Gamma - 1)} = \frac{\alpha w_B - 2}{\alpha + 2}, \tag{12}$$

where $\Gamma \equiv 1 + \frac{1}{\alpha} > 1$ from Eq. (6) for the IPL potential, and $w_B$ is the equation of state of the fluid component dominating the background. So, during the era of radiation domination, with $w_B = \frac{1}{3}$,

$$w_\phi = \frac{\alpha - 6}{3(\alpha + 2)}, \tag{13}$$

and during the era of matter domination, with $w_B = 0$,

$$w_\phi = \frac{-2}{\alpha + 2}. \tag{14}$$

We also note here that, as in the case of all tracker potentials, the tracker solution for the IPL model is approached differently for different initial conditions. For example, in what is referred to as the "overshoot" case, $\rho_{\phi,I}$ begins from a value greater than the tracker solution value. Assuming that $\phi$ is released from rest, the dynamics of the scalar field starts with an early kinetic phase ($\dot{\phi}^2 \gg V$) in which $w \to 1$ so that $\rho_\phi \propto a^{-6}$ [from Eq. (11)] and $V$ decreases very rapidly as $\phi$ runs downhill. Since the kinetic energy is too large for $\phi$ to join the tracker solution as $\phi$ rolls further down the potential, $\phi$ will overshoot the tracker solution. The field will then freeze (as will $V$ and $\frac{V'}{V}$) as $w_\phi$ rushes towards $-1$. Finally, when $\phi$ rejoins the tracker solution, $\phi$ will run downhill again and $w_\phi$ will increase from $-1$, briefly oscillate, and then settle into the tracker value [18].

In the "undershoot" case, $\rho_{\phi,I}$ begins from a value much smaller than the tracker solution value, and $\phi$ is once again released from rest. This corresponds to the kinetic energy density being very small and $\phi$, $V$, and $\frac{V'}{V}$ being approximately constant or "frozen" as the universe evolves. Then, as in the overshoot case, $w_\phi$ reaches close to $-1$, $\rho_\phi \approx$ const, and $\rho_B$ is decreasing. The value of $w_\phi$ then increases from $-1$ as $\phi$ once again runs downhill. After a few oscillations, $w_\phi$ will then rejoin the tracker solution until $\rho_\phi$ becomes the dominant component in the universe.

Figures 2–4 depict the evolution of $w_\phi$ for the IPL model during these various regimes. With little sensitivity to the

exact value of $V_0$, $\alpha$ will determine the amplitude of the $w$ curve and the value of $w_0 \equiv w(z=0) \gtrsim -1$ as long as $\phi_I \ll M_P$. For given values of $\alpha$, $\phi_I$ determines when the scalar field joins the tracker solution and how long it follows the tracking solution (Fig. 3). As is pointed out in [28], we also find that for the smaller values of $\alpha$ that we focus on in this work (e.g., $\alpha \lesssim 1$), the smaller $\alpha$ is, the later the tracker is reached for a given initial value of $\phi$ (Fig. 4). With regards to $V_0$, we find that while increasing (decreasing) the value of $V_0$ leads to corresponding increases (decreases) in $\omega_{\rm DE} = \frac{\rho_\phi}{\rho_c} h^2$ at $z = 0$ (where $h = \frac{H_0}{100}$), as expected, it leads to very small (essentially negligible) decreases (increases) in the value of $w_0$ and essentially no change in the tracking solutions or tracking behavior. When the scalar field has tracking solutions, different values of $\phi_I$ lead to similar values of, for example, $-0.9 > w_0 > -1$, with $w \to -1$ and $\Omega_m \to 0$ as $a \to \infty$. There will be essentially no dependence of $\phi_I \ll M_P$ on either the present dark energy equation of state or the present contribution of dark energy to the total energy density of the universe (as illustrated in Fig. 3).

### C. The nontracking case

It is possible to find nontracking cosmological solutions for IPL quintessence. If $\phi_I \sim M_P$, then $\phi$ will follow the tracker solution for only a very brief period of time or not exhibit tracking behavior at all. In our computational algorithms, for example, we find that tracking solutions do not strictly exist and thus tracking behavior does not strictly occur for, roughly, all $\phi_I \gtrsim 10^{-5}$ when $\alpha \lesssim 1$ and $0.25 \lesssim V_0 \lesssim 0.45$. Moreover, for some instances in which $-1.5 \lesssim \log_{10}(\phi_I) \lesssim -0.3$, $w \approx -1$ initially but then increases towards $-1 > w_0 > -0.9$, for example, as for the case of thawing models and behaviors [27,29,30]. Examples of this nontracking thawing-like behavior of the equation of state for $\phi_I = 10^{-1}$ for $\alpha = 0.2$ and 0.1 can also be seen (dashed-dotted curves) in Figs. 2 and 3. Nontracking initial conditions for the IPL model as well as possible connections between the quintessence field and the inflation field (the inflaton) [31], which are beyond the scope of this work, are discussed in some detail in [32] and references therein. Like [32], and as we discuss further in Sec. IV B, we also find that for cases where $\phi_I \to M_P$ and the field has not joined the tracker by the present epoch, the range of acceptable values of $\alpha$ increases significantly as $w$ increases. For values of $\log_{10}(\phi_I)$ roughly between $-5$ and $-1$, $w_\phi$ leaves its tracking phase with matter and enters a transient phase (see Fig. 3) before exhibiting thawing behavior for $\log_{10}(\phi_I) \gtrsim -1.5$.

### D. The transition from tracking to acceleration

For most of this work, we focus on cosmological solutions that exhibit tracking at early times. Out of respect for big bang nucleosynthesis [33] and other standard considerations, there must be an early epoch of radiation domination where $\rho_\phi \ll \rho_r$ and redshifts as [1,34]

$$\rho_\phi \propto a^{-(4\alpha/(2+\alpha))}. \tag{15}$$

It is possible in this case to find an exact solution to the Klein-Gordon equation for which

$$\phi \propto a^{4/(2+\alpha)}, \tag{16}$$

and it can be shown that this solution is an attractor [1]. During matter domination, the attractor is also characterized by the scalar field evolving as

$$\phi \propto a^{3/(2+\alpha)}, \tag{17}$$

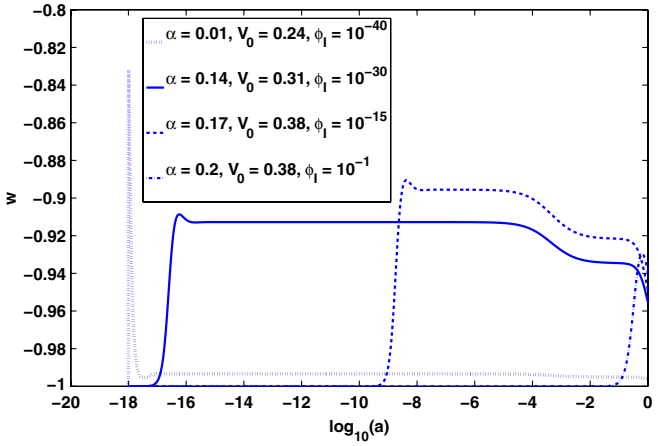


FIG. 2 (color online). An illustration of how the evolution and tracking behavior of $w$ as a function of the scale factor $a$ is affected by different values of $\alpha$, $V_0$, and $\phi_I$. The $a$ scale is logarithmic here in order to show behavior on all time scales.

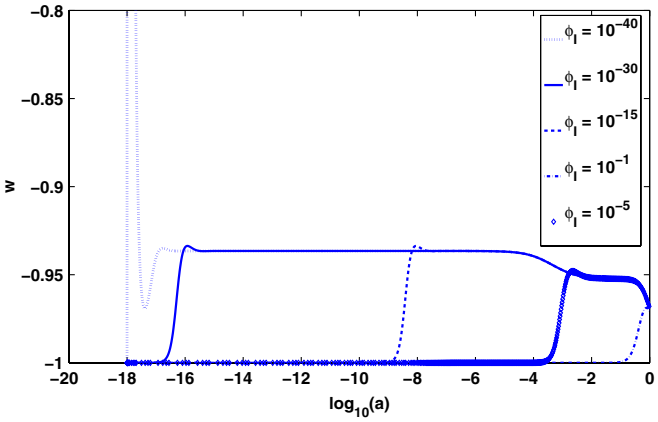


FIG. 3 (color online). Examples of how the evolution and tracking behavior of $w$ as a function of the scale factor $a$ is affected by different values of $\phi_I$ for given values of $V_0$ and $\alpha$. For all curves, $V_0 = 0.38$ and $\alpha = 0.1$. These examples illustrate how different values of $\phi_I$ lead to the same values of the equation-of-state parameter today. The $a$ scale is logarithmic here in order to show behavior on all time scales.

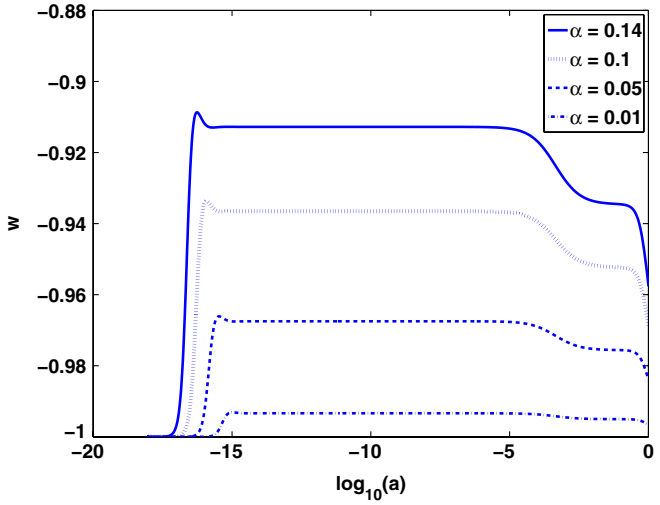


FIG. 4 (color online). This figure depicts the evolution and tracking behavior of $w$ as a function of the scale factor $a$ for different values of $\alpha$ for given values of $V_0 = 0.38$ and $\phi_I = 10^{-30}$. As long as $\phi_I \ll M_P$, $\alpha$ will determine $w_0$ and the amplitude of the $w(a)$ curves. In addition, the smaller $\alpha$ is, the later the tracker is reached for a given $\phi_I$. The $a$ scale is logarithmic here in order to show behavior on all time scales.

corresponding to energy density evolving as

$$\rho_\phi \propto a^{-(3\alpha/(2+\alpha))}. \tag{18}$$

As long as $\frac{\rho_\phi}{\rho_m} \ll 1$, these expressions provide a very good approximation to the behavior of the IPL quintessence field [19,35]. In other words, the tracking regime itself is strictly valid only when the expansion of the universe is dominated by matter. Then, at later times, when $\rho_\phi$ starts to make a significant contribution to the cosmic expansion rate, the value of $w_\phi$ in Eq. (12) starts to diverge from its tracker value, as do $\phi(a)$ and $\rho_\phi(a)$, such that the scalar field mimics the behavior of a cosmological constant today (with $w \approx -1$), consistent with current observations. So, we can see that $\rho_\phi$ in the attractor solution decreases less quickly than $\rho_m$ and $\rho_r$, which allows us to realize the following behavior: Deep in the era of radiation domination, $\rho_\phi$ is small enough to satisfy constraints from standard models for big bang nucleosynthesis and the formation of the light elements, but $\rho_\phi$ does eventually become large enough today (with $w \rightarrow -1$) so that the universe undergoes accelerated expansion and acts as if it has a cosmological constant, but one that slowly varies with time and position [36].

### E. Current constraints

From an observational standpoint, if we require $w_0$ to be roughly consistent with current observational constraints, say, for example, $-1 \lesssim w \lesssim -0.8$ [37–40], then the power law index $\alpha$ must be roughly in the range $0 \lesssim \alpha \lesssim 0.5$, yielding a shallow potential shape. The quintessence equation of state in the current epoch abandons the tracking regime because the dark energy is now the dominant component. However, the shallow potential shape makes $w_0$ not far from the tracking one in Eq. (14), differing typically at the 10% level [26,41].

Various combinations of data [including CMB, baryon acoustic oscillation (BAO), type Ia supernovae (SNe Ia), and weak gravitational lensing (WL) observations] have been used to constrain the slope of the IPL potential, finding $\alpha \lesssim 1$–2 (e.g., [24,42–55]), so that flatter potentials seem to be favored by the data. Recently, for example, Ref. [43] found $0.7 \lesssim \alpha \lesssim 0.8$ in an MCMC analysis of the IPL potential when assuming that the energy scale of the potential is that of a cosmological constant (i.e., $V_0 \approx \Lambda^4 \approx 10^{-47}$ GeV$^4$), $\Omega_\phi = \frac{\rho_\phi}{\rho_c}$ varies in the range 0.1–0.9, and $h = 0.70$. In many instances our combinations of stage 2 simulated data sets (see Sec. IV) place substantially tighter constraints on $\alpha$ than do real data sets used by various authors in their analyses of the IPL model (e.g., [48–55]). A number of authors (e.g., [33,56,57]) have argued that such small values of $\alpha$ lead to smaller basins of attraction and thus some degree of fine-tuning and dependence on initial conditions for the IPL model. We have observed, however, that for the realistic cosmologies that we consider for this work, there remains a substantial basin of attraction: We can vary the initial conditions over a very large range of values with the end results for $\Omega_{\phi,0}$, for example, still being physically acceptable [57].

Other authors (e.g. [17,18,57]) have also explored a variety of issues associated with tracking properties and solutions for this model. They considered theoretical constraints relating to, for example, equipartition initial conditions between quintessence and the remaining fluid components which argue for larger values of $\alpha$ [18,32]. However, in our work we have focused for the most part on realistic families of cosmological solutions that are broadly consistent with observational constraints (i.e., $\alpha \lesssim 1$) and which also include IPL tracking properties and behaviors that give the model its conceptual appeal. We also note that [24] has found that, while $\alpha$ is tightly constrained, IPL models with $0.25 \lesssim \Omega_m \lesssim 0.4$ remain viable, and [48–51] have recently shown that various sets and combinations of data can not yet completely rule out slowly evolving dark energy described by the IPL model.

The real appeal of IPL models from our point of view is that they offer an interesting class of non-$\Lambda$ cosmologies with some degree of theoretical motivation. Thorough discussions of the basin of attraction (as well as the still outstanding cosmological constant problem) are key to a fundamental understanding of the ultimate importance one might give to the IPL model. We regard such discussions as too poorly developed at this point to give them much weight in the very phenomenological analysis in this paper. For our purposes, it is good enough that a large range of initial conditions can converge to a common solution,

thereby avoiding to a substantial degree the fine-tuning of initial values of $\frac{\rho_\phi}{\rho_B}$ and $w_\phi$ [32].

## III. PARAMETRIZATION OF THE INVERSE POWER LAW MODEL

As a general rule, MCMC analysis requires a careful choice of the model parameters to be varied. Poor parameter choices and degeneracies between parameters can slow the rate of convergence and mixing of the Markov chain, reducing the overall efficiency by which the Markov chain explores a parameter space. For the IPL potential, $V = V_0(\frac{M_P}{\phi})^\alpha$, the obvious choices of potential parameters to be varied are $\phi_I$, $\alpha$, and $V_0$. When we carried out our MCMC analysis of data forecast by the DETF to constrain the IPL quintessence model around a fiducial $\Lambda$CDM model, we chose our fiducial value for $V_0$ (in units of $h^2$) to be 0.38, which is the value of the dark energy density today for a cosmological constant. We chose to make $V_0$ a model parameter in our MCMC analysis rather than keeping it fixed because other choices of $V_0$ could provide equivalent cosmological solutions, and we were also interested in ascertaining how the MCMC exploration of the parameter space and its ability to constrain the other parameters would be affected by varying $V_0$ as well.

We have not found a need to reparametrize the IPL parameters to the extent that has been done, for example, in [5,6] for the Albrecht-Skordis or exponential potential quintessence models. We did, however, find it necessary to place bounds on some of the potential parameters in order to prevent the MCMC algorithm from infinitely stepping into divergent directions of parameter space and thus never converging to a stationary probability distribution. Another reason we placed bounds on the potential parameters was to prevent the MCMC algorithm from spending possibly large amounts of computer time exploring uninteresting regions of parameter space that may be completely inconsistent with observational and theoretical constraints.

We placed a lower bound of 0 on $\alpha$, as $\alpha > 0$ is required for the pure IPL model that we consider [22]. Given that the DETF data used in the first part of our MCMC analysis are modeled around a cosmological constant, the most probable values of $\alpha$ will be those in which $\alpha$ approaches zero. From Eq. (7) we see that as $\phi_I \rightarrow M_P$ any value of $\alpha$ will lead to the same value of the potential $V(\phi)$ for a given $V_0$. However, since $\alpha$ largely controls the shape of the potential [as well as the amplitude of $w(a)$] and thus the evolution of the dark energy density and $w_{\phi,0}$, we find that the simulated data sets place sufficient constraints on $\alpha$ to prevent the MCMC chain from infinitely stepping into divergent directions in the $\alpha - \phi_I$ and $V_0 - \phi_I$ parameter spaces, even when $\phi_I \rightarrow M_P$. This renders a stringent upper bound on $\alpha$ unnecessary.

We can also see from Eq. (7) that $\phi_I$ can take on any value and lead to solutions indistinguishable from a cosmological constant as $\alpha \rightarrow 0$. This degeneracy leads to a divergent direction in the $\alpha - \phi_I$ space, where $\phi_I$ can be arbitrarily large or small. Also, the simulated data sets do not constrain $\phi_I$ nearly as tightly as $\alpha$ due to the fact (previously discussed in the context of attractor solutions) that a broad range of $\phi_I$ values can lead to the same $\phi_0$ and $w_0$ and thus have little effect on the evolution of the dark energy density. Because of this effect, it is necessary to choose some cutoffs on $\phi_I$ so that these infinite directions are bounded.

As discussed in Sec. II B we have parametrized our potential in a way that gives cosmologically realistic solutions where $V(\phi)$ approaches the value of the dark energy density today when $\phi \approx M_P$. With this in mind, we impose an upper bound of $M_P$ on $\phi_I$ which helps avoid solutions with uninterestingly low values of $\rho_\phi$ as well as solutions that are dominated by transients. We also note here that, given that the main thrust of our work involves an MCMC analysis of the regions of parameter space associated with tracking, we have selected or filtered out nontracking parameter values in the algorithms used to generate likelihood contours from the MCMC chains by implementing in our algorithms the criteria for tracking solutions (as discussed in Secs. II A and II B) and, specifically, the "equation of motion" discussed in [18]. Thus, all of the error contours displayed and discussed in Secs. IV B and IV B correspond to portions of the parameter space associated with tracking (i.e., parameter values corresponding to attractor solutions of the Klein-Gordon equation). Incidentally, we have found that for a typical stage 2 MCMC chain generated from a $\Lambda$CDM model, for example, about 90% of points stepped to by the chain correspond to parameters with tracker solutions, whereas the other 10% correspond to nontracking (transient and thawing) parameters.

Regarding a lower bound on $\phi_I$, we recall from Sec. II B that we must have $\phi_I \ll M_P$ so that the present field value, $\phi_0$ (of order $M_P$), is reached from a very broad range of initial conditions. This ensures that the tracking properties and solutions that make this model appealing are still included and valid within the parameter space explored in our MCMC analysis. If the lower bound on $\phi_I$ is too large, $\phi_I$ may reach the tracking phase only at very late times or only by the present time (or not at all), leading to a small basin of attraction and fine-tuning problems. We find that placing a lower bound of $\phi_I = 10^{-20}$ in our MCMC analysis gives reasonable results by ensuring that, on the one hand, the tracking solutions and properties are included in the parameter space explored by the MCMC analysis (i.e., there is a larger basin of attraction and $\phi_0 \approx M_P$) but, on the other hand, an appropriate cutoff or bound has been placed on a divergent direction in the $\alpha - \phi_I$ space that may not otherwise be constrained by the data (and thus possibly preventing the MCMC chains from coming to equilibrium).

The above lower bound is not well suited for examining the finer details of nontracking transient and thawing regions of parameter space (where $\phi_I \rightarrow M_P$). In chains with a lower bound of $10^{-20}$ or smaller on $\phi_I$, the part ( $\approx 10\%$) of the chain that shows nontracking and thawing IPL solutions is not sufficiently well populated to show the full structure of the probability distribution. In order to allow the MCMC algorithm to step more frequently in these parameter space regions and so better converge (as discussed in [4]) on a well-resolved probability distribution for the nontracking and thawing regions of the parameter space, we have also carried out an MCMC analysis with a lower bound of $-3$ placed on $\log_{10}(\phi_I)$ [see Sec. IV D].

## IV. MCMC RESULTS AND ANALYSIS

### A. General approach

Following the approach taken by the DETF, we generated ''data models'' or simulated data sets for future SNe Ia, BAO, WL, and CMB (PLANCK) observations. These considerations of DE projects follow developments in ''stages'': Stage 2 represents ongoing projects that are relevant to dark energy; stage 3 consists of medium-cost, near-term, currently proposed projects (such as BAO, SNe Ia, and WL surveys with 4-meter class telescopes using photometric redshifts); stage 4 consists of the Joint Dark Energy (Space) Mission, Square Kilometer Array, and/or Large Survey Telescope (LST) [8]. ''Optimistic'' and ''pessimistic'' versions of the same data models give different estimates of systematic errors. Additional information on the specific DETF data models is given in Appendix A of [4] and the technical appendix of the DETF report [8]. We excluded the DETF galaxy cluster data models in our work because the extension of the DETF calculations to our analysis is not straightforward, especially in regards to estimates of systematic errors [4–6,58].

We have generated two sets of data models. One type is generated around a cosmology with a cosmological constant, consistent with DETF stage 2, 3, and 4 SNe Ia, WL, BAO, and CMB data models. The other set of data models is built around an IPL fiducial model which was chosen to be consistent with simulated stage 2 data based on a cosmological constant cosmology. We then use a MCMC algorithm to map the likelihood around each fiducial model ($\Lambda$CDM and IPL) via a Markov chain of points in parameter space, starting with the fiducial model and moving to a succession of random points in space using a Metropolis-Hastings stepping algorithm. The technical details of our MCMC algorithm are presented in Appendix B of [4] and references therein. In this way we can, for example, analyze the parameter space of IPL quintessence in the light of DETF data models and evaluate the likelihood function of the parameters of our model. Once the Markov chains of our models in parameter space have been computed, we can extract likelihood contours from the distribution of models and display them as projected 2D likelihood contour plots. This can then give us a picture of the shape of the likelihood region of all the parameters in our models in the whole multidimensional parameter space if we were to plot likelihood contours for each pair of parameters in the parameter space. In all plots in this paper, we show 68.27% ($1\sigma$), 95.44% ($2\sigma$), and 99.73% ($3\sigma$) confidence contours, which consist of points where the likelihood equals $e^{-(2.30/2)}$, $e^{-(6.17/2)}$, and $e^{-(11.8/2)}$ of the maximum value of the likelihood, respectively. We have constructed these plots by marginalizing over all of the cosmological parameters, $\omega_m$, $\omega_k$, $\omega_B$, $\omega_r$, $h$, $\delta_\zeta$, $n_s$, $n_s'$ (as defined by the DETF), and the various nuisance and/or photometric redshift parameters, which take into account uncertainties and errors in the simulated data. The nuisance and photometric redshift parameters are described and explained in detail in [4,8].

### B. Cosmological constant fiducial model

In this section we present the results of our MCMC analysis for the combined simulated data sets generated around a $\Lambda$CDM cosmology. We list the values of the free parameters for our $\Lambda$CDM fiducial model (with energy density and $V_0$ in units of $h^2$ and $\phi_I$ in reduced Planck units) in Table I. (The IPL parameters given generate a cosmological constant.)

We note that $h^2(a=1) = \omega_m + \omega_r + \omega_k + \omega_{\rm DE}$, with recent observations providing a prior constraint of $h = 0.72 \pm 0.008$ [59]. Also, $\omega_r$, the radiation energy density, is not a free parameter for our calculations but is fixed by the CMB temperature (and the standard assumption of three massless neutrinos) [8].

Stage 2 combines SNe Ia, WL, and CMB data models but does not include BAO data models. Stages 3 and 4 additionally include the BAO data models as well. As discussed in Sec. IV A we project our probability distributions into 2D spaces given by pairs of the IPL parameters (i.e., the $V_0 - \alpha$, $V_0 - \phi_I$, and $\phi_I - \alpha$ planes).

The likelihood contours in the $V_0 - \alpha$ plane, with all nontracking parameter values [$\log_{10}(\phi) \lesssim -6$] excluded,

TABLE I. Fiducial parameter values (energy densities in units of $h^2$) for the $\Lambda$CDM model.

| | |
|---|---|
| $\omega_{\rm DE}$ | 0.3796 |
| $\omega_m$ | 0.146 |
| $\omega_k$ | 0.0 |
| $\omega_B$ | 0.024 |
| $\omega_r$ | $4.16 \times 10^{-5}$ |
| $n_s$ | 1.0 |
| $n_s'$ | 0.000 01 |
| $\delta_\xi$ | 0.87 |
| $h$ | 0.72 |
| $\alpha$ | 0.0 |
| $\phi_I$ | $10^{-15}$ |
| $V_0$ | 0.38 |

for stage 2 and the optimistic versions of stage 3 photometric, stage 4 space, and stage 4 ground LST combined data are shown in Fig. 5. In all cases the error contours show the expected trend of the IPL potential to approach a cosmological constant as $\alpha \to 0$ (and also corresponding to where the slope of the potential goes to 0). The vertical axis where $\alpha = 0$ corresponds to $\Lambda$. Therefore, the value of $V(\phi_0) = V_0$ on the vertical axis represents $\Lambda$ or the dark energy density $\omega_{\rm DE}$ for $\alpha = 0$. However, along the lines of the discussion in Sec. III of [6] for the Albrecht-Skordis model and as discussed in this paper in Sec. II B, we must also keep in mind that the parameter $V_0$ does not have a significant effect on the equation of state of dark energy. Moreover, for $\alpha > 0$, $V_0$ is no longer identical to $\omega_{\rm DE,0} \equiv \omega_{\rm DE}(z = 0)$.

For small values of $\alpha$, there is a spread in $V_0$ in the $V_0 - \alpha$ space. Since these values of $\alpha$ are consistent with $\Lambda$ or a nonevolving dark energy, the spread in $V_0$ is essentially a measure of how well the experiments are measuring $\omega_{\rm DE,0}$. The spread or uncertainty in $V_0$ for all $\alpha$ is also a result of uncertainties on measurements of $\Omega_{m,0}$. Larger values of $\alpha$ correspond to larger values of $w (w > -1)$ and thus values of $w$ that deviate more and more from the equation of state for $\Lambda$ as $\alpha$ increases, possibly up to values of $\alpha$ that correspond to detectable differences from $\Lambda$. The smallest values of $V_0$ correspond to the largest values of $\alpha$, which in turn correspond to the largest values of the equation of state (and hence those values of $w$ deviating the most from what we expect for a cosmological constant). As the value of $\alpha$ increases, we see that the likelihood contour in Fig. 5 has an overall downward curved shape. This is due to the fact that the slope of the potential becomes steeper for increasing values of $\alpha$, which leads to greater evolution of the dark energy density and larger values of $w_0$ that deviate more and more from $-1$. The reduction in the $V_0$ direction reflects improving constraints with increasing stage number on the dark energy density. As a specific quantitative example of this, we see from the stage 4 error contours in Fig. 5 that the extrema of the range of $V_0$ values deviate from the fiducial value by less than 20% when $\alpha \approx 0.1$ and by less than 5% when $\alpha \approx 0$. The shrinking in the $\alpha$ direction corresponds to increasing constraints on deviations from a cosmological constant.

Figure 6 depicts likelihood contours in $V_0 - \log_{10}(\phi_I)$ space, where, again, all nontracking transient and thawing parameter values have been removed. As noted in Sec. III, we imposed $10^{-20} < \phi_I/M_P < 1$. Since a large range of initial values of the scalar field ($\phi_I < M_P$) are generally washed out by the tracking behavior, we can see from the contours that there is very little dependence of the dark energy density today on $\phi_I \ll M_P$. Once again, the spread in $V_0$ values is essentially a measure of how well the experiments are measuring the dark energy density at the present time. The error contours also show a slight trend toward an increasing range of acceptable values of $\phi_I$ which possess attractor solutions as $V_0$ decreases, which is associated with greater $\alpha$ values and thus greater dark energy evolution. The sections of the overall parameter space depicted in these figures also tend to disfavor larger values of $\alpha$, or, equivalently, disfavor larger departures from a cosmological constant and thus more dark energy evolution. We once again note a reduction in the $V_0$ direction with increasing stage number, indicating the improving constraints that the data place on the dark energy contribution to the total energy density of the universe today.

The likelihood contours in the $\log_{10}(\phi_I) - \alpha$ (Fig. 7) space are clearly seen to shrink in the $\alpha$ direction with increasing stage number, once again showing improving constraints on the amount of dark energy evolution and on deviations from a cosmological constant from stage 2 to stage 3 and from stage 3 to stage 4. This corresponds to a greater disfavoring of larger values of $\alpha$ with successive

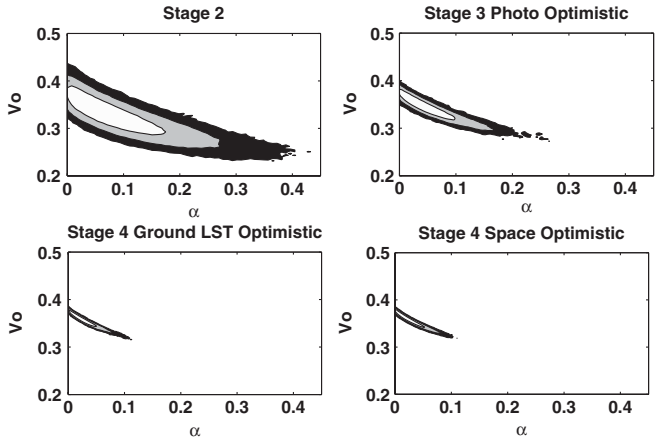


FIG. 5. $V_0 - \alpha$ $1\sigma$ (68.27%), $2\sigma$ (95.44%), and $3\sigma$ (99.73%) confidence regions for DETF optimistic combined $\Lambda$CDM data models.

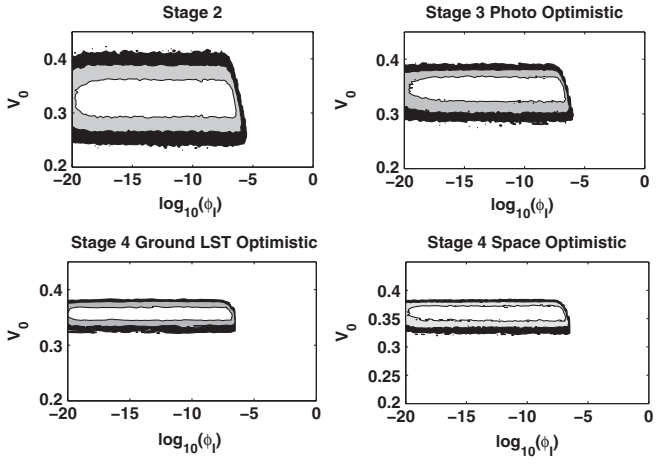


FIG. 6. $V_0 - \log_{10}(\phi_I)$ $1\sigma$ (68.27%), $2\sigma$ (95.44%), and $3\sigma$ (99.73%) confidence regions for DETF optimistic combined $\Lambda$CDM data models.

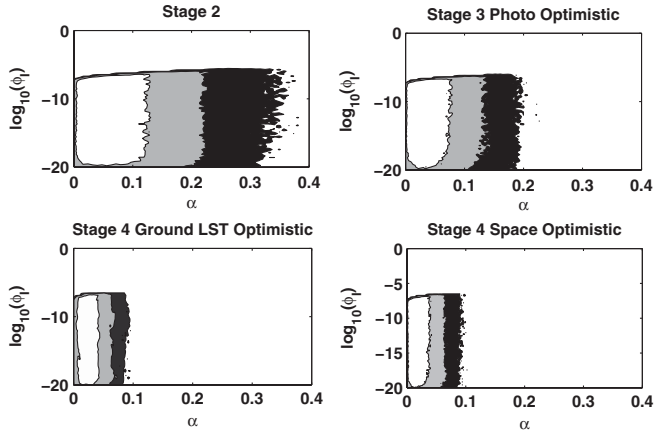


FIG. 7. $\log_{10}(\phi_I) - \alpha$ $1\sigma$ (68.27%), $2\sigma$ (95.44%), and $3\sigma$ (99.73%) confidence regions for DETF optimistic combined ΛCDM data models.

stages of data. We also see in Fig. 7 a very slight trend toward an increasing range of acceptable values of $\phi_I$ possessing attractor solutions as $\alpha$ increases. This corresponds to the trend of a larger range and upper limit for $\phi_I$ having attractor solutions for smaller values of $V_0$ discussed in regards to Fig. 6.

The trend described above in Fig. 7 is related to the fact that the largest values of $\phi_I$, from which the attractor is joined before the present time, occur on the flatter portions of the potential where $w_\phi$ is closer to $-1$ in recent times and today, and the curvature and slope of the potential are smaller. Since $\alpha$ controls the steepness of the potential, changes in $\alpha$ have less of an effect on the flatter parts of the potential where $\phi_I$ is larger and $V(\phi_I)$, $V(\phi_I)'$, and $V(\phi_I)''$ are smaller [as can also be seen in Eqs. (8)–(10)]. So, when the scalar field tracks the background evolution on flatter portions of the potential, we expect a slight increase in the range of acceptable (tracking) $\phi_I$ values as $\alpha$ increases.

Overall, as found by the DETF, successive stages of data do better at constraining the evolution of dark energy. As can be seen in the likelihood contours above and as was also found for the case of the Albrecht-Skordis model [6], the IPL potential parameters appear to be somewhat better constrained by the DETF stage 4 LST ground data models than by the DETF stage 4 space data models. This reflects the fact that ground and space data are sensitive to slightly different features of the dark energy evolution.

### C. Inverse power law fiducial model

We next evaluate the power of future experiments by assuming that the dark energy in the universe can actually be described by the inverse power law model rather than a ΛCDM fiducial model. For our fiducial IPL model, we use $\alpha = 0.14$, $\phi_I = 10^{-15}$, and $V_0 = 0.31$. The remaining parameters of the IPL fiducial model are the same as those used in the fiducial ΛCDM model. Our IPL model fiducial values (given in Table II with energy densities and $V_0$ in units of $h^2$ and $\phi_I$ in reduced Planck units) were chosen, excluding consideration of the thawing or outlying regions of the parameter space, to lie near the boundary of (or just beyond) $1\sigma$ detection or within the 95.44%($2\sigma$) confidence region in the $V_0 - \alpha$ and $\log_{10}(\phi_I) - \alpha$ spaces (Figs. 5 and 7) for stage 2 ΛCDM data, but excluded by more than $3\sigma$ in the stage 4 optimistic ground and space data so as to be strongly ruled out by stage 4 ΛCDM data.

TABLE II. Fiducial parameter values (energy densities in units of $h^2$) for the inverse power law model.

| | |
|---|---|
| $\omega_{\rm DE}$ | 0.3796 |
| $\omega_m$ | 0.146 |
| $\omega_k$ | 0.0 |
| $\omega_B$ | 0.024 |
| $\omega_r$ | $4.16 \times 10^{-5}$ |
| $n_s$ | 1.0 |
| $n_s'$ | 0.000 01 |
| $\delta_\xi$ | 0.87 |
| $h$ | 0.72 |
| $\alpha$ | 0.14 |
| $\phi_I$ | $10^{-15}$ |
| $V_0$ | 0.31 |

We also ensured that this fiducial model had initial conditions and had an equation of state such that the attractor is joined before the present time. The equation-of-state parameter as a function of scale factor $a$ for all time scales (the $a$ scale is logarithmic) for our fiducial model is similar to the dashed curves in Figs. 2 and 3. We also depict the potential of the fiducial model in the top panel of Fig. 8, along with the corresponding equation-of-state evolution as a function of redshift in the bottom panel. The fiducial model corresponds to the point $w_0 = -0.955$, which deviates from $w(z) = -1$ by only about 4.5%. We have chosen our fiducial model to thus be marginally consistent with the ΛCDM-based data but demonstrating sufficient dark energy evolution to be different enough from Λ to be resolved by stage 4 experiments. In this way we are able to illustrate the power of stage 4 data models and their ability to rule out the Λ model.

Duplicating our MCMC analysis methods for the IPL fiducial model, we again marginalized over all but two pairs of the parameters $\alpha$, $\phi_I$, and $V_0$ for the purposes of generating 2D likelihood regions for the IPL dark energy parameters. Figure 9 shows the results of our MCMC analysis and calculations for stage 2, stage 3 photo-optimistic, stage 4 LST optimistic, and stage 4 space optimistic data models in the $V_0 - \alpha$ parameter space. We can see from the $\alpha = 0$ axis, corresponding to a cosmological constant, that the ΛCDM model (i.e., a non-evolving scalar field) is still allowed at stage 2 [at the $2\sigma$ (95.44%) confidence level but not quite at the $1\sigma$ (68.27%) confidence level] but becomes less favored by subsequent stages of data models. At stage 3 the ΛCDM model lies

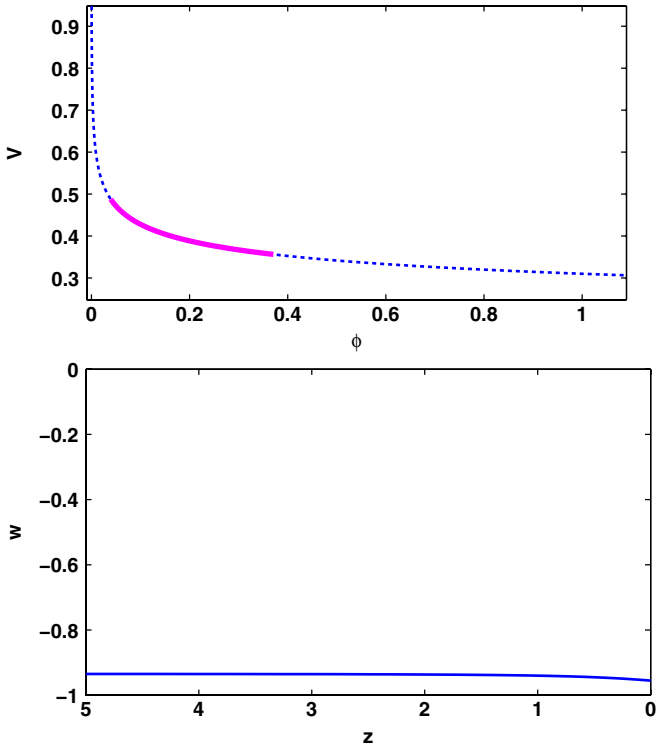


FIG. 8 (color online). The potential of the IPL fiducial model ($\alpha = 0.14$, $\phi_I = 10^{-15}$, $V_0 = 0.31$) (top panel, dashed curve). The corresponding equation-of-state evolution $w(z)$ for a potentially observable range of redshift values is shown in the bottom panel. The solid curve overlaying the potential in the top panel shows the evolution of the IPL fiducial model scalar field for the range of $z$ values (from $z = 5$ to the present time) depicted for $w(z)$ in the bottom panel.

outside of the $2\sigma$ contour, and by stage 4 it is ruled out by well over $3\sigma$. For stage 2 and subsequent stages, the range of $\alpha$ values covered by the contours is significantly greater than for the $\Lambda$CDM case since dark energy solutions with more evolution are favored more here. The greater dark energy evolution for this case also leads to the slightly more significant downward trend in the shape of the contours than is seen in the $\Lambda$CDM confidence contours.

The described increase in constraining power for higher quality data models is similar to the $\Lambda$CDM results in Sec. IV B for the $\Lambda$CDM model. However, as previously indicated, the range of $\alpha$ values has significantly increased within the $1\sigma$, $2\sigma$, and $3\sigma$ contours, allowing for an increased range of evolving dark energy solutions. From the stage 4 combined data sets, we can clearly differentiate between our selected IPL fiducial model and the $\Lambda$CDM model by well over $3\sigma$. This increased constraining power is again consistent with the ($\Lambda$CDM) DETF results for stage 4 experiments. Hence, the results of our MCMC analysis, as seen in Fig. 9 (as well as Fig. 11 below), show that, for a universe described by this specific IPL fiducial model, the stage 4 experiments will rule out a cosmological constant by well over $3\sigma$.

Figure 10 shows likelihood contours in $V_0 - \log_{10}(\phi_I)$ space. As for the case of the $\Lambda$CDM model, there is again very little dependence of dark energy density today on $\phi_I$ when $\phi_I \ll M_P$. Once again, the spread in $V_0$ values is essentially a measure of how well the experiments are measuring the present dark energy density as given by the chosen IPL fiducial model. The trend toward an increasing range of and acceptable upper limit to values of $\phi_I$ possessing attractor solutions for smaller $V_0$, as noted in reference to Fig. 6, is slightly more pronounced here due to the larger range of acceptable values of $\alpha$ and greater DE evolution for the IPL model.

The likelihood contours in the $\log_{10}(\phi_I) - \alpha$ (Fig. 11) plots are clearly seen to shrink in the $\alpha$ direction with increasing stage number, but the overall range of $\alpha$ values stepped to by the MCMC chain and thus included within

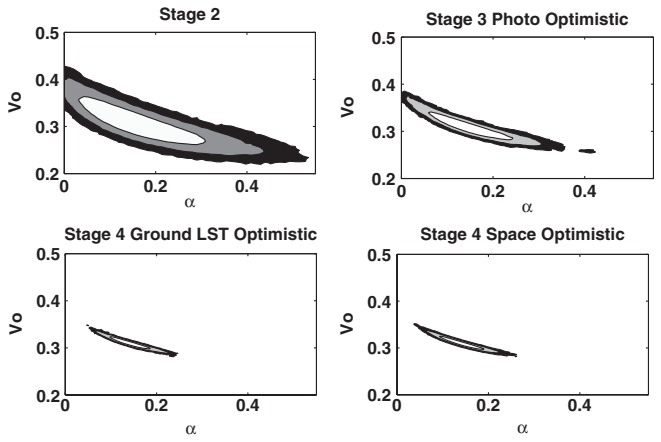


FIG. 9. $V_0 - \alpha$ $1\sigma$ (68.27%), $2\sigma$ (95.44%), and $3\sigma$ (99.73%) likelihood contours for DETF optimistic combined data sets generated from a selected IPL background cosmological model.

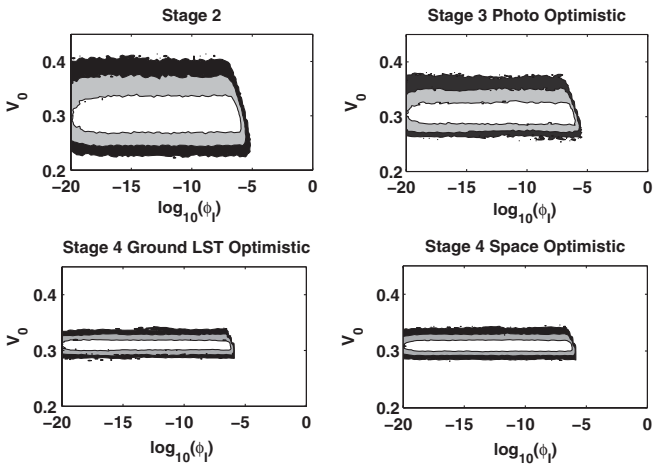


FIG. 10. $V_0 - \log_{10}(\phi_I)$ $1\sigma$ (68.27%), $2\sigma$ (95.44%), and $3\sigma$ (99.73%) likelihood contours for DETF optimistic combined data sets generated from a selected IPL background cosmological model.

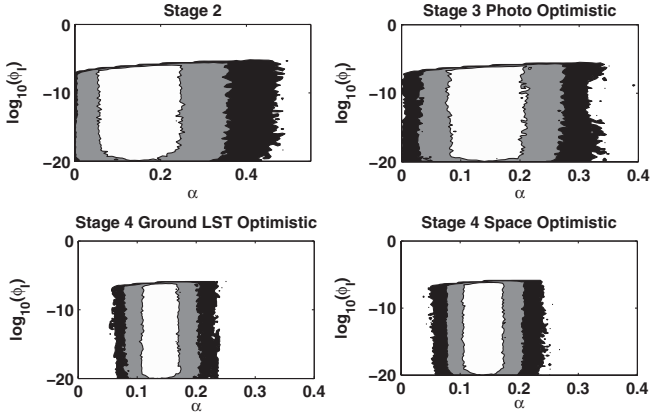


FIG. 11. $\log_{10}(\phi_I) - \alpha$ $1\sigma$ (68.27%), $2\sigma$ (95.44%), and $3\sigma$ (99.73%) likelihood contours for DETF optimistic combined data sets generated from a selected IPL background cosmological model.

the likelihood contours is significantly larger than for the $\Lambda$CDM model data sets, again indicating that dark energy solutions with more evolution are disfavored less for this IPL fiducial model than for the $\Lambda$CDM model. The $\log_{10}(\phi_I) - \alpha$ contours also show [like the $V_0 - \log_{10}(\phi_I)$ contours in Fig. 10] that the $\Lambda$CDM model is still allowed at stage 2 (but lies just outside of the $1\sigma$ contour) and at stage 3 photo-optimistic (lying outside of the $2\sigma$ contour here) but is ruled out by well over $3\sigma$ by stage 4, again becoming less favored by subsequent stages of data sets. We also see a slightly more pronounced trend of an increasing range of acceptable values of $\phi_I$ possessing attractor solutions as $\alpha$ increases. Again, this corresponds to the increasing range of acceptable $\phi_I$ values possessing attractor solutions for smaller $V_0$ in Fig. 10 and the fact that the part of the IPL potential where the largest values of $\phi_I$ that lead to attractor solutions that are still acceptable is steeper (larger $\alpha$) than for the $\Lambda$CDM case [Eqs. (8)–(10)].

As in the case of the $\Lambda$CDM data sets discussed in Sec. IV B and found in the Albrecht-Skordis model [6], we find once again that stage 4 ground data (this time based on our fiducial IPL model) constrain the parameters $\alpha$ and $V_0$ slightly more strongly than the stage 4 space data do. This is the opposite of what has been found with other scalar field models [4,5].

### D. Nontracking parameter space regions

Though the main focus of our work has involved an analysis of the tracking regions of the parameter space of the IPL model, here we discuss briefly the results of our MCMC analysis of the nontracking regions, i.e., initial values of the scalar field from which the attractor is *not* joined before or by the present time. In this case, our motivation is simply to explore an interesting-looking class of dark energy behaviors that have already been considered elsewhere in the literature (e.g., [32]). We acknowledge that to the extent that the tracking behavior is a key reason to consider the IPL model, the solutions considered in this section do not benefit from the same degree of motivation.

As indicated previously, in order to allow the MCMC algorithm to step more frequently in nontracking portions of the parameter space and so bring out greater detail in the thawing and some of the transient portions, we have also generated MCMC chains with a lower bound of $-3$ placed on $\log_{10}(\phi_I)$. These outlying regions of parameter space associated with the thawing equation-of-state behavior (again corresponding to $\phi_I \rightarrow M_P$ and increasing $w$ and present-day dark energy density values in recent times) can clearly be seen in the stage 2 and stage 3 error contours for our IPL fiducial model depicted in Fig. 12 at $\alpha \gtrsim 0.5$, where the contours turn or ''flare'' upward and become more ''patchy.''. This unsmooth and flared appearance of the $2\sigma$ and $3\sigma$ contours corresponds to the largest values of $\phi_I$, where the equation of state $w(a)$ increases or does not turn down as steeply near scale factors of unity and so is exhibiting thawing-like behavior; therefore, the acceptable range of $\alpha$ values significantly increases as $w$ increases.

These portions of the likelihood contours correspond to outlier points lying relatively far outside the main distribution of parameter points stepped to by the MCMC chain. In these regions of parameter space the scalar field starts to evolve on the flatter portions of the IPL potential where $V(\phi_I)$ is small. We see that there is a greater spread in $V_0$ values, and, thus, $V_0$ is less constrained by the data here. This is again related to the fact that the corresponding equation-of-state values for $\phi_I \sim M_P$ do not turn down as steeply near scale factors of unity (or even increase towards values greater than $-1$) compared to $w$ values corresponding to $\phi_I < M_P$. We can see that the area of

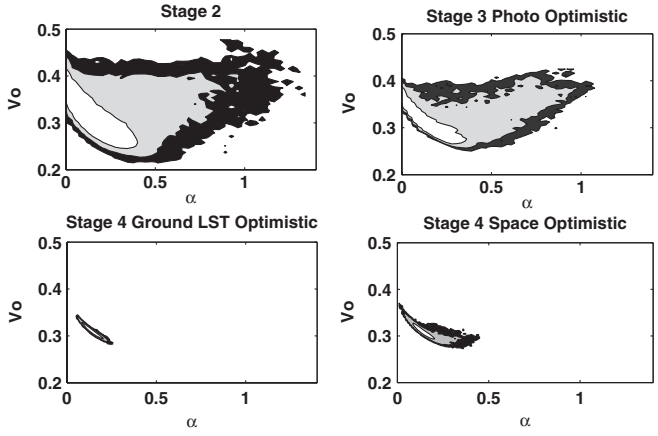


FIG. 12. $V_0 - \alpha$ $1\sigma$ (68.27%), $2\sigma$ (95.44%), and $3\sigma$ (99.73%) likelihood contours for DETF optimistic combined data sets generated from a selected IPL background cosmological model for the case of a cutoff of $\log_{10}(\phi_I) = -3$ placed on the MCMC algorithm. This effectively gives an enlarged and more detailed view of nontracking and thawing-like regions of the parameter space.

these outlying likelihood contours shrinks and tightens from stage 2 to stage 3 and again from stage 3 to stage 4. The reduction in the $V_0$ direction again shows the improving constraints that the higher quality data place on these outlying transient and thawing regions. We also observe an apparent illustration here of the ability of the stage 4 ground-based simulated data sets to better constrain the thawing behavior than the stage 4 space-based data. This appears to be consistent with the results obtained in the MCMC analysis for the tracking regions of parameter space. Moreover, the stage 4 space-based data rule out a significant portion of the thawing region of the parameter space, while the stage 4 ground LST optimistic data sets appear to rule out nearly all of the thawing parameter values.

Figure 13 depicts $\log_{10}(\phi_I) - \alpha$ likelihood contours for our IPL fiducial model for nontracking regions of parameter space associated with transient and outlying thawing equation-of-state behavior. Given that our MCMC analysis does not focus nearly as much on nontracking regions of parameter space than on the tracking regions, our chains may not have equilibrated for the nontracking regions to the same extent as they have done for tracking regions. However, we believe that important trends can still be ascertained from this analysis. In the stage 2 and stage 3 likelihood contours, a significant increase in the $\alpha$ direction for the largest $\phi_I$ values ($\phi_I \rightarrow M_P$) can be seen. This corresponds to the fact, as discussed in Sec. II B, that for the IPL model the range of acceptable $\alpha$ values is largest for the largest initial scalar field values from which the attractor is not joined by the present time. This is associated with the flatter part of the IPL potential that is less sensitive to $\alpha$, which controls the slope of the potential.

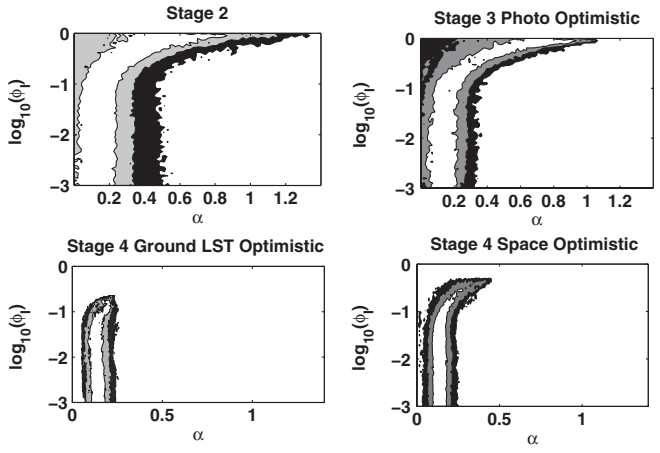


FIG. 13. $\log_{10}(\phi_I) - \alpha$ $1\sigma$ (68.27%), $2\sigma$ (95.44%), and $3\sigma$ (99.73%) likelihood contours for DETF optimistic combined data sets generated from a selected IPL background cosmological model for the case of a cutoff of $\log_{10}(\phi_I) = -3$ placed on the MCMC algorithm. This effectively gives an enlarged and more detailed view of nontracking and thawing-like regions of the parameter space.

As can be seen from Eq. (9), flatter parts of the potential correspond to cases where $V(\phi_I) \sim V(\phi_0)$ is small and $\phi_I$ is large. Thus, even large values of $\alpha$ can be associated with flatter portions of the potential here. So, as long as $V(\phi_I) \sim V(\phi_0)$ remains very small and the ratio of $\alpha$ and $\phi_I$ does not become too large, a larger range of acceptable values of $\alpha$, leading to similar cosmologies, will be allowed within the parameter space. Moreover, larger $\phi_I$ values combined with larger $\alpha$ can lead to similar $w(a) \gtrsim -1$ with behavior close to that of $\Lambda$. Hence, for stage 3 data and especially stage 4 data, the MCMC chain will not step as much in this region (since $\Lambda$CDM models and models with similar behavior are ruled out to a greater extent by stage 3 and stage 4 data). This explains the greater constraints placed in the $\alpha$ direction for the very largest $\phi_I$ values for successive stages of data sets, and is consistent with the overall trend of the likelihood contours in the $\log_{10}(\phi_I) - \alpha$ space shrinking in the $\alpha$ direction with higher quality data.

The extent to which larger $\alpha$ values (and thus significant portions of the thawing regions of the parameter space) are constrained and even ruled out by the stage 4 data sets also reflects the degree to which evolving dark energy is constrained and disfavored by the higher quality data sets. Once again, and perhaps more dramatically illustrated here, we see that the ground-based stage 4 data sets constrain the thawing regions of parameter space for the IPL model to a more significant extent than do the stage 4 space-based data sets.

## V. DISCUSSION AND CONCLUSIONS

We have presented our MCMC analysis of the inverse power law quintessence model using combined simulated data sets forecast by the DETF and representing future dark energy experiments. In doing so, we have analyzed the impact of DETF simulated data models in the context of the IPL model of dark energy and demonstrated the ability of these experiments to place significant constraints on the parameters of a quintessence model. We have found that the effect of the DETF combined data models on the parameter space of IPL models is broadly consistent with the DETF findings. In particular, we have found a significant improvement in the constraining power of each successive stage of DETF simulated data sets.

We have shown likelihood contours for choices of combined DETF data sets and found the increase in IPL dark energy parameter constraints with increasing data quality to be consistent with the DETF results in the $w_0 - w_a$ parameter space. For example, the relative constraints on the size of the $V_0 - \phi_I$ parameter space between different simulated data sets lead to similar constraints computed by the DETF in the $w_0 - w_a$ parameter space. A direct comparison with the DETF figure of merit was complicated by the fact that the IPL model depends on three parameters ($\alpha$,

$\phi_I$, and $V_0$), while the DETF FoM was calculated based on the two-dimensional $w_0 - w_a$ space. However, we found that the changes in the areas of projected two-dimensional likelihood contours were consistent with the DETF results. Specifically, the DETF reported a FoM (defined as the inverse area inside the 95% likelihood contours in the $w_0 - w_a$ plane) that showed a gain of at least a factor of 3 in going from stage 2 to good combinations of stage 3 data sets (and thus roughly a factor of 3 decrease in the allowed parameter area when moving from stage 2 to good combinations of stage 3 data), and a gain of at least a factor of 10 in going from stage 2 to good combinations of stage 4 data. We observed decreases by similar amounts in our projected 2D likelihood contours for pairs of IPL parameters.

In the course of this work we have also produced and examined similar 2D likelihood plots of a much wider range of combined DETF simulated data sets, including data models with pessimistic estimates of systematic errors and data models representing single DE observing techniques. We found our results in the IPL model parameter space to be consistent with the constraints reported by the DETF in the $w_0 - w_a$ space across the complete range of data combinations and selections that we considered.

We constructed our simulated data sets from two different background cosmologies, one with a cosmological constant and one with an IPL scalar field with specific parameter values. We found our results to be consistent with those of the DETF in both cases. We have separately analyzed cases constrained to having early tracking behavior and other cases which focused on the nontracking solutions. In each case we have placed bounds on some of the IPL potential parameters as necessary to prevent the MCMC algorithm from infinitely stepping in divergent directions of parameter space (and thus never converging to a stationary probability distribution) and to also enable us to better examine and analyze details in enlarged regions of parameter space corresponding to nontracking behavior.

In order to demonstrate the power stage 4 experiments will have for detecting the evolution of dark energy, we chose a specific background IPL scalar field model, with parameter values of $\alpha = 0.14$, $\phi_I = 10^{-15}$, and $V_0 = 0.31$, that was consistent with stage 2 data based on a cosmological constant. This specific model corresponds to $w(a = 1) \equiv w_0 = -0.955\,35$, which deviates from $w = -1$ by about 4.5%. One must look back to much earlier times (e.g., $a < 0.2$) and/or look to larger $\alpha$ parameter values in order to find more significant deviation from $w = -1$ for this quintessence model (see Figs. 1–4). We found that if the universe were in fact to be described by this fiducial IPL quintessence model, then good stage 4 experiments would rule out a $\Lambda$CDM model by better than $3\sigma$, indicating that there is indeed a dynamical component to dark energy. For the IPL background cosmology, we found that the $\Lambda$CDM model lies outside the $1\sigma$ contour but within the $2\sigma$ contour at stage 2 and lies outside of the $2\sigma$ likelihood contour by stage 3. We also noted that the variable $\alpha$ was somewhat more strongly constrained by stage 4 ground data sets than with stage 4 space data. This is consistent with the results reported by [6] for a similar MCMC analysis carried out on the Albrecht-Skordis scalar field model, but is opposite to the behavior displayed by the exponential and pseudo-Nambu-Goldstone-boson scalar field models as described in our other companion papers [4,5]. This effect is currently under investigation and may lead to new insights into the complementarity of ground- and space-based stage 4 dark energy projects.

We have found, as also discussed in [2] and demonstrated in our companion papers [4–6], that widely varying families of functions $w(a)$ for the IPL model are constrained by the DETF data sets in a similar way to the constraints found in the $w_0 - w_a$ parameter space by the DETF. In particular, we have seen that the main IPL model potential parameter $\alpha$ is constrained by DETF data models in a comparable way to the constraints found in the $w_0 - w_a$ formulation by the DETF, even though the $w_0 - w_a$ parameters describe very different functions $w(a)$. We believe that this relates to the fact pointed out in [58] that high quality DETF data sets will be able to constrain many more properties of $w(a)$ that are present in the $w_0 - w_a$ parametrization alone and will thus be able to make good measurements of significantly more than two equation-of-state parameters. More specifically, by considering the IPL family of $w(a)$ functions and the $w_0 - w_a$ family of functions in terms of an orthonormal basis of independently measured mode functions $w_j(a)$ (as discussed in [2,13,58]), we are able to ensure that a wide variety of different $w(a)$ functions will be constrained as well as the DETF $w_0 - w_a$ parameters. In other words, the various quintessence models (discussed in this paper and in our companion papers) are just sampling different random combinations of the ''well measured modes'' discussed in [13,58] and, in each case, lead to similar results. This also appears to reflect the fact that many more functions $w(a)$ are measured than are contained in any of the quintessence model $w(a)$ family of functions alone [6]. Consequently, modeling the impact of future dark energy experiments using the two-parameter DETF scheme makes some sense in that it gives a good indicator of the impact of scalar field dark energy models with a similar number of parameters in the quintessence potential.

One of the advantages of the techniques employed in this work and the companion work [4–6] is that we can explicitly examine how simulated data sets representing future dark energy experiments can constrain actual theoretically motivated quintessence models (in addition to abstract parametrizations such as the $w_0 - w_a$ ansatz) in a significant way. As developed further in [7], this approach helps us understand how future data have the capability to reject some (or possibly even all) current dark energy models entirely.

## ACKNOWLEDGMENTS

We would like to thank David Ring for useful discussions, technical assistance, and for finding an error in our code. We also acknowledge Tony Tyson and his group for the use of their computer cluster, and, in particular, Perry Gee and Hu Zhan for their expert advice and computing support. We also thank Gary Bernstein for providing us with Fisher matrices suitable for adapting the DETF weak lensing data models to our methods. This work was supported in part by DOE Grant No. DE-FG03-91ER40674 and NSF Grant No. AST-0632901.

[1] B. Ratra and P. J. E. Peebles, Phys. Rev. D **37**, 3406 (1988).
[2] A. Albrecht, AIP Conf. Proc. **957**, 3 (2007).
[3] R. Bousso, Gen. Relativ. Gravit. **40**, 607 (2008).
[4] A. Abrahamse, A. Albrecht, M. Barnard, and B. Bozek, Phys. Rev. D **77**, 103503 (2008).
[5] B. Bozek, A. Abrahamse, A. Albrecht, and M. Barnard, Phys. Rev. D **77**, 103504 (2008).
[6] M. Barnard, A. Abrahamse, A. Albrecht, B. Bozek, and M. Yashar, Phys. Rev. D **77**, 103502 (2008).
[7] M. Barnard, A. Abrahamse, A. Albrecht, B. Bozek, and M. Yashar, Phys. Rev. D **78**, 043528 (2008).
[8] A. Albrecht *et al.*, arXiv:astro-ph/0609591.
[9] M. Chevallier and D. Polarski, Int. J. Mod. Phys. D **10**, 213 (2001).
[10] E. V. Linder, Phys. Rev. Lett. **90**, 091301 (2003).
[11] R. de Putter and E. V. Linder, J. Cosmol. Astropart. Phys. 10 (2008) 042.
[12] A. R. Liddle, P. Mukherjee, D. Parkinson, and Y. Wang, Phys. Rev. D **74**, 123506 (2006).
[13] A. J. Albrecht *et al.*, arXiv:0901.0721.
[14] D. Huterer and H. V. Peiris, Phys. Rev. D **75**, 083503 (2007).
[15] M. J. Mortonson, W. Hu, and D. Huterer, Phys. Rev. D **79**, 023004 (2009).
[16] E. J. Copeland, M. Sami, and S. Tsujikawa, Int. J. Mod. Phys. D **15**, 1753 (2006).
[17] I. Zlatev, L.-M. Wang, and P. J. Steinhardt, Phys. Rev. Lett. **82**, 896 (1999).
[18] P. J. Steinhardt, L. Wang, and I. Zlatev, Phys. Rev. D **59**, 123504 (1999).
[19] A. R. Liddle and R. J. Scherrer, Phys. Rev. D **59**, 023509 (1998).
[20] P. J. Steinhardt, Phys. Scr. **T117**, 34 (2005).
[21] A. Masiero, M. Pietroni, and F. Rosati, Phys. Rev. D **61**, 023504 (1999).
[22] P. J. E. Peebles and B. Ratra, Astrophys. J. **325**, L17 (1988).
[23] J. Martin, Mod. Phys. Lett. A **23**, 1252 (2008).
[24] R. R. Caldwell and M. Doran, Phys. Rev. D **69**, 103517 (2004).
[25] M. Eriksson and R. Amanullah, Phys. Rev. D **66**, 023530 (2002).
[26] F. Giovi, C. Baccigalupi, and F. Perrotta, Phys. Rev. D **68**, 123002 (2003).
[27] R. R. Caldwell and E. V. Linder, Phys. Rev. Lett. **95**, 141301 (2005).
[28] M. Malquarti and A. R. Liddle, Phys. Rev. D **66**, 023524 (2002).
[29] R. J. Scherrer, Phys. Rev. D **73**, 043502 (2006).
[30] R. J. Scherrer and A. A. Sen, Phys. Rev. D **77**, 083515 (2008).
[31] M. C. Bento, R. G. Felipe, and N. M. C. Santos, Phys. Rev. D **77**, 123512 (2008).
[32] J. P. Kneller and L. E. Strigari, Phys. Rev. D **68**, 083517 (2003).
[33] M. Yahiro, G. J. Mathews, K. Ichiki, T. Kajino, and M. Orito, Phys. Rev. D **65**, 063502 (2002).
[34] P. Brax and J. Martin, Phys. Rev. D **61**, 103502 (2000).
[35] C. R. Watson and R. J. Scherrer, Phys. Rev. D **68**, 123524 (2003).
[36] P. J. E. Peebles and B. Ratra, Rev. Mod. Phys. **75**, 559 (2003).
[37] P. Astier *et al.* (SNLS), Astron. Astrophys. **447**, 31 (2006).
[38] D. N. Spergel, R. Bean, O. Doré, M. R. Nolta, C. L. Bennett, J. Dunkley, G. Hinshaw, N. Jarosik, E. Komatsu, L. Page *et al.*, Astrophys. J. Suppl. Ser. **170**, 377 (2007).
[39] A. G. Riess *et al.*, Astrophys. J. **659**, 98 (2007).
[40] M. Kowalski *et al.*, Astrophys. J. **686**, 749 (2008).
[41] C. Baccigalupi, A. Balbi, S. Matarrese, F. Perrotta, and N. Vittorio, Phys. Rev. D **65**, 063520 (2002).
[42] L. Amendola and C. Quercellini, Phys. Rev. D **68**, 023514 (2003).
[43] L. P. L. Colombo and M. Gervasi, J. Cosmol. Astropart. Phys. 10 (2006) 001.
[44] G. Barro Calvo and A. L. Maroto, Phys. Rev. D **74**, 083519 (2006).
[45] C. Schimd *et al.*, Astron. Astrophys. **463**, 405 (2007).
[46] C. Schimd and I. Tereno, J. Phys. A **40**, 7105 (2007).
[47] G. Efstathiou, Mon. Not. R. Astron. Soc. **388**, 1314 (2008).
[48] L. Samushia and B. Ratra, arXiv:0806.2835.
[49] L. Samushia and B. Ratra, Astrophys. J. **680**, L1 (2008).
[50] L. Samushia and B. Ratra, arXiv:0810.2104.
[51] L. Samushia, G. Chen, and B. Ratra, arXiv:0706.1963.
[52] L. Samushia and B. Ratra, Astrophys. J. **650**, L5 (2006).
[53] K. M. Wilson, G. Chen, and B. Ratra, Mod. Phys. Lett. A **21**, 2197 (2006).
[54] G. Chen and B. Ratra, Astrophys. J. **612**, L1 (2004).
[55] K.-H. Chae, G. Chen, B. Ratra, and D.-W. Lee, Astrophys. J. **607**, L71 (2004).
[56] S. Bludman, Phys. Rev. D **69**, 122002 (2004).
[57] A. de la Macorra and C. Stephan-Otto, Phys. Rev. D **65**, 083520 (2002).
[58] A. Albrecht and G. Bernstein, Phys. Rev. D **75**, 103003 (2007).
[59] W. L. Freedman *et al.*, Astrophys. J. **553**, 47 (2001).